Supporting Information

Versatile Template-Free Construction of Hollow Nanostructured CeO_2 Induced by Functionalized Carbon Materials

Zhi-Jia Sun[a], Hao Ge*[a], Shuai Zhu[a], Xiao-Man Cao[a], Xin Guo[a], Zhong-Hai Xiu[a], Zi-Hang Huang[ab], Hui Li[ab], Tianyi Ma*[c], Xi-Ming Song*[a]

[a] Liaoning Key Laboratory for Green Synthesis and Preparative Chemistry of Advanced Materials, College of Chemistry, Liaoning University, Shenyang 110036 P. R. China.

[b] Institute of Clean Energy Chemistry, Liaoning University, Shenyang 110036 P. R. China.

[c] Discipline of Chemistry, University of Newcastle, Callaghan, NSW, 2308 Australia, tianyi.ma@newcastle.edu.au.

Supplementary Figures

Fig. S1 TG curve of HS-CeO_2/MWCNTs.

Fig. S2 SEM (a) and TEM (b) images of CeO_2 nanoparticles.

Fig. S3 XPS full spectra of CeO_2 nanoparticles (a) and high-resolution XPS spectra of C 1s (b), O 1s (c) and Ce 3d (d) for CeO_2 nanoparticles.

Fig. S4 Fabrication procedures of CeO_2 nanoparticles (a); CeO_2/bare MWCNTs (b); HS-CeO_2/MWCNTs (c) and CeO_2-coated MWCNTs (d).

Fig. S5 Comparison of the specific capacitances of CeO_2 nanoparticles, CeO_2/bare MWCNTs, HS-CeO_2/MWCNTs and CeO_2-coated MWCNTs electrodes at different current densities.

Fig. S6 Survey scan of different MWCNTs (a); XPS C1s spectra of different MWNTs (b). MWCNTs treated for 1 and 12 h are named as SMMWCNTs-1 and SMMWCNTs-24, respectively.

Fig. S7 Raman spectra of different MWCNTs. MWCNTs treated for 1 and 12 h are named as SMMWCNTs-1 and SMMWCNTs-24, respectively.

Fig. S8 FT-IR spectra of different MWCNTs. MWCNTs treated for 1 and 12 h are named as SMMWCNTs-1 and SMMWCNTs-24, respectively.

Fig. S9 Morphologies of hollow sphere CeO_2/carbon composites. SEM images of hollow sphere CeO_2/activated carbon (a) and hollow sphere CeO_2/graphene oxide (b).

Fig. S10 SEM image of hollow sphere Fe_2O_3/MWCNTs (a) and TEM image of hollow sphere Fe_2O_3/MWCNTs; XRD diffraction patterns of MWCNTs and HS-Fe_2O_3/MWCNTs (c). The inset image of (a) shows broken hollow sphere Fe_2O_3.

Fig. S11 TEM images of HS-CeO_2/MWCNTs formed in the early periods (a) and HS-CeO_2/MWCNTs (b).

Fig. S12 Galvanostatic charge-discharge profiles of CeO_2 nanoparticles at different current densities.

Fig. S13 CV curves of CeO_2 nanoparticles (a); graphs of lower anodic peak currents plotted against $v^{1/2}$ for HS-CeO_2/MWCNTs and CeO_2 nanoparticles (b); graphs of higher anodic peak currents plotted against v for HS-CeO_2/MWCNTs and CeO_2 nanoparticles (c).

Fig. S14 Capacitive contribution of CeO_2 nanoparticles at 10 mV s^{-1}.

Fig. S15 Rate performance of HS-CeO_2/MWCNTs and CeO_2 nanoparticles.

Fig. S16 The simulation equivalent circuit for the the Nyquist plots of HS-CeO_2@MWCNTs and CeO_2 nanoparticles.

Fig. S17 Schematic representation of the device.

Fig. S18 CV curves of AC at the scan rate of 100 mV s^{-1} (a); galvanostatic charge-discharge profiles of AC at 1 A g^{-1} (b).

Fig. S19 CV curves of HS-CeO_2/MWCNTs//AC all-solid ASC at various scan rates.

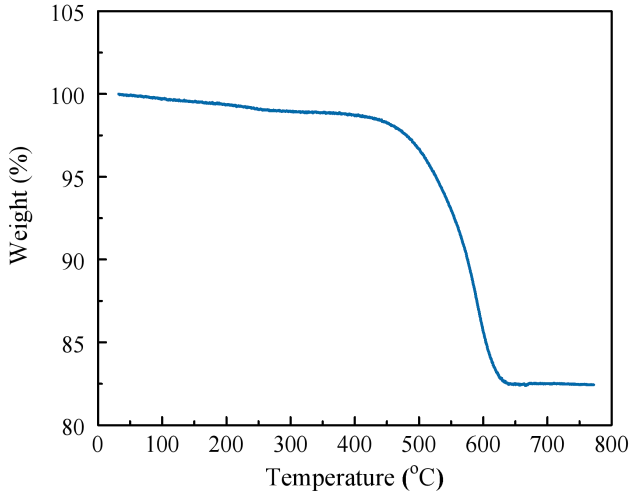

Fig. S1 TG curve of HS-CeO_2/MWCNTs.

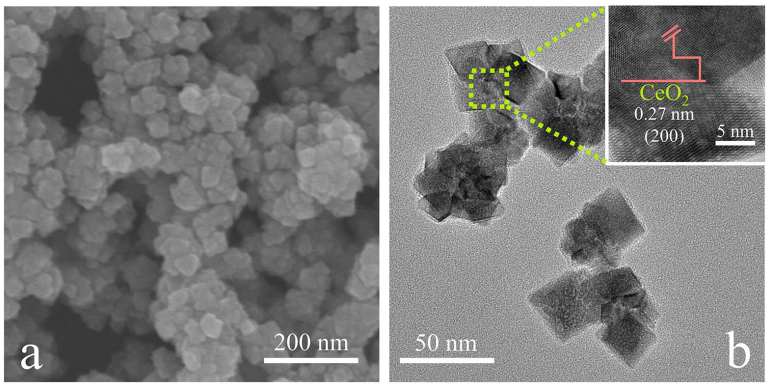

Fig. S2 SEM (a) and TEM (b) images of CeO_2 nanoparticles.

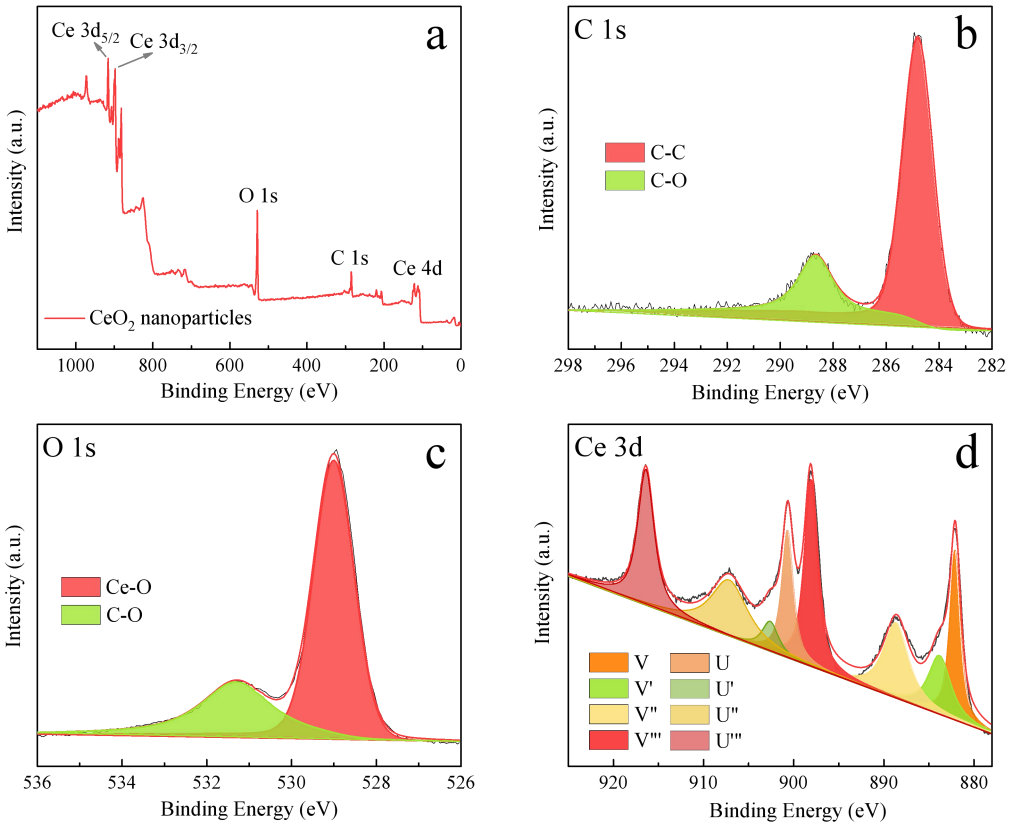

Fig. S3 XPS full spectra of CeO_2 nanoparticles (a) and high-resolution XPS spectra of C 1s (b), O 1s (c) and Ce 3d (d) for CeO_2 nanoparticles.

The concentration of the O_{sur} can be estimated using the following equation:

$$\frac{[O_{sur}]}{[O_{sur}+O_{lat}]}=\frac{area(O_{sur})}{total\cdot area} \quad (1)$$

According to equation 1, the O_{sur} value of HS-CeO_2/MWCNTs (45.62%) is much higher than that of CeO_2 nanoparticles (25.77%), indicating the presence of abundant adsorbed surface oxygen on HS-CeO_2/MWCNTs. The higher O_{sur} value reveals the larger amount of oxygen vacancies in HS-CeO_2/MWCNTs and suggests that the HS-CeO_2/MWCNTs composite possesses higher electrochemistry activity[1].

By deconvolution of Ce^{3+} and Ce^{4+} in Ce 3d spectrum, the concentration of Ce^{3+} in the composites can be calculated using the following equation:

$$\frac{[Ce^{3+}]}{[Ce^{3+}+Ce^{4+}]}=\frac{area(v',u')}{total\cdot area} \quad (2)$$

The higher Ce^{3+} concentration (21.85%) after the introduction of MWCNTs indicates that HS-CeO_2/MWCNTs contains much higher density of electrochemical active sites compared with CeO_2 nanoparticles (13.1%). The higher Ce^{3+} concentration can effectively catalyze the redox reaction of Ce^{3+}/Ce^{4+} and enhance the bulk conductivity[2], which is highly desirable for the materials' electrochemical applications.

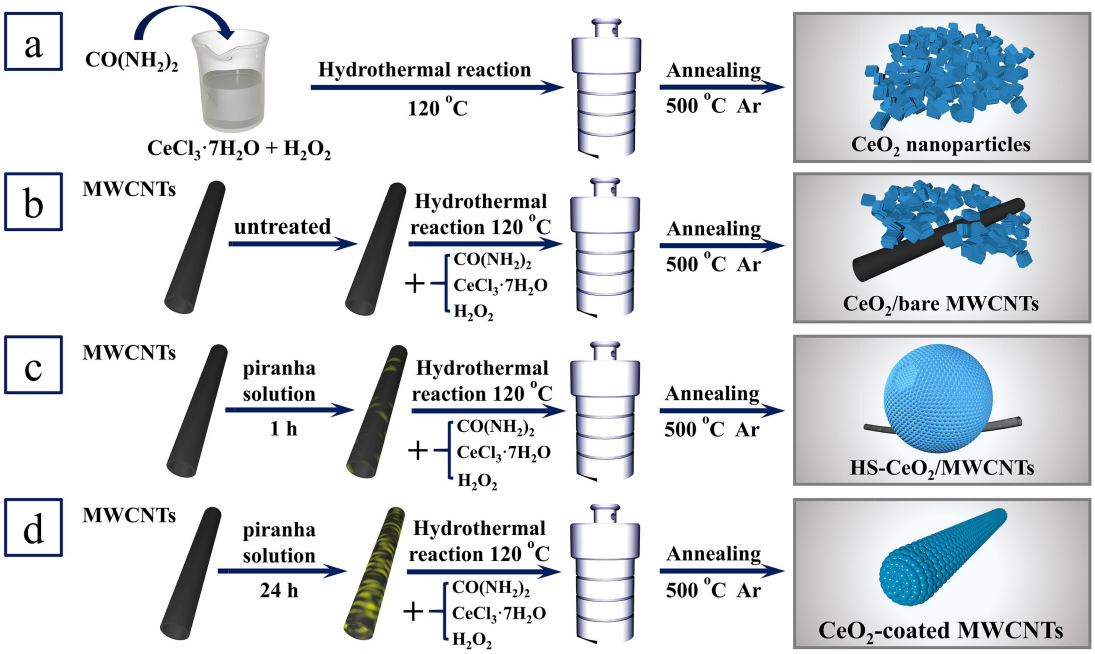

Fig. S4 Fabrication procedures of CeO_2 nanoparticles (a); CeO_2/bare MWCNTs (b); HS-CeO_2/MWCNTs (c) and CeO_2-coated MWCNTs (d).

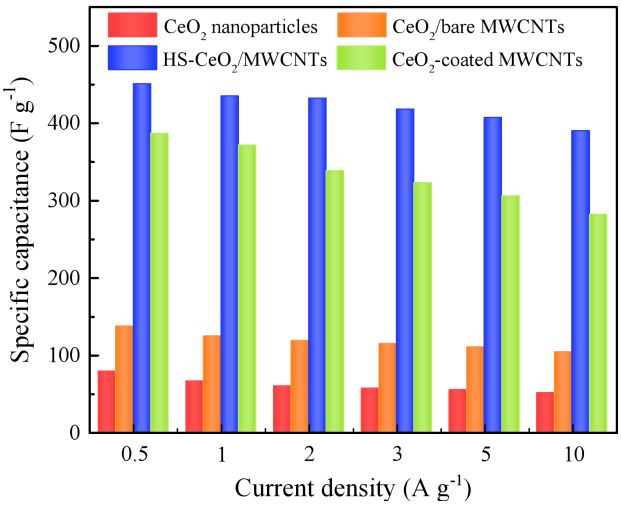

Fig. S5 Comparison of the specific capacitances of CeO_2 nanoparticles, CeO_2/bare MWCNTs, HS-CeO_2/MWCNTs and CeO_2-coated MWCNTs electrodes at different current densities.

.

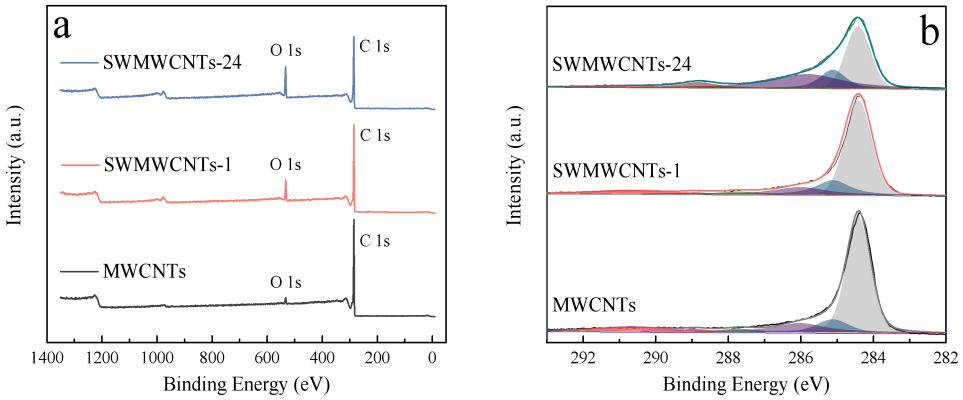

Fig. S6 Survey scan of different MWCNTs (a); XPS C1s spectra of different MWNTs (b). MWCNTs treated for 1 and 12 h are named as SMMWCNTs-1 and SMMWCNTs-24, respectively.

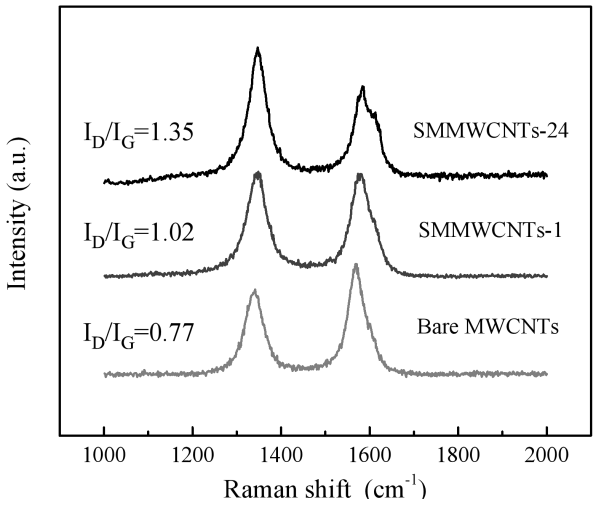

Fig. S7 Raman spectra of different MWCNTs. MWCNTs treated for 1 and 12 h are named as SMMWCNTs-1 and SMMWCNTs-24, respectively.

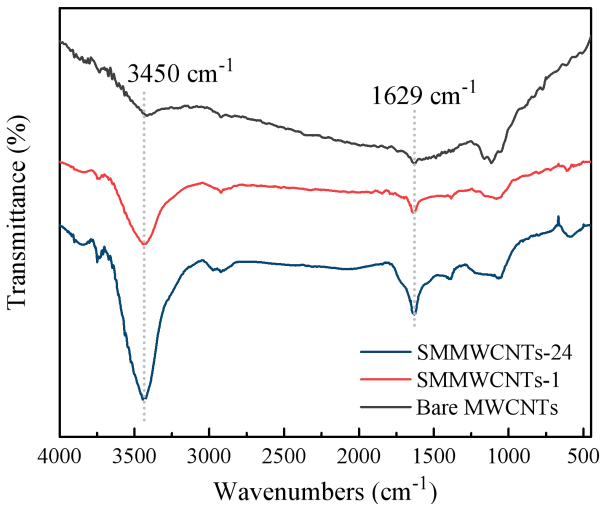

Fig. S8 FT-IR spectra of different MWCNTs. MWCNTs treated for 1 and 12 h are named as SMMWCNTs-1 and SMMWCNTs-24, respectively.

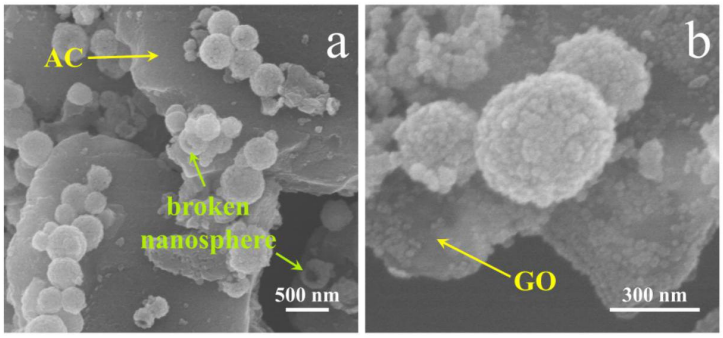

Fig. S9 Morphologies of hollow sphere CeO_2/carbon composites. SEM images of hollow sphere CeO_2/activated carbon (a) and hollow sphere CeO_2/graphene oxide (b).

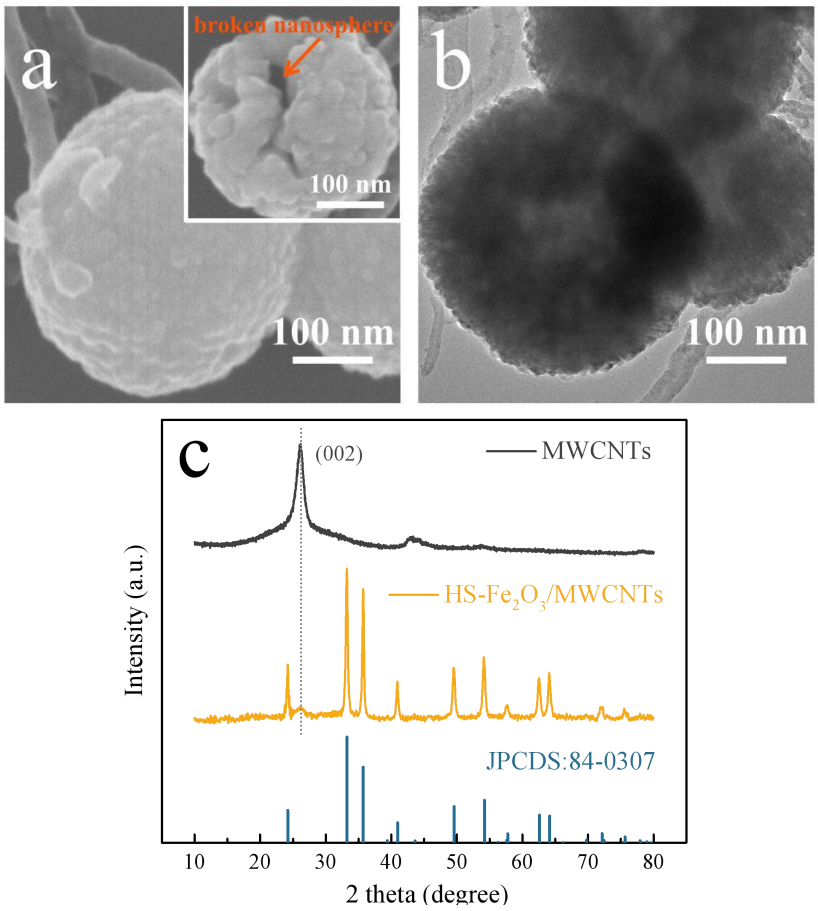

Fig. S10 SEM images of hollow sphere Fe_2O_3/MWCNTs (a) and TEM image of hollow sphere Fe_2O_3/MWCNTs (b); XRD diffraction patterns of MWCNTs and HS-Fe_2O_3/MWCNTs (c). The inset image of (a) shows broken hollow sphere Fe_2O_3.

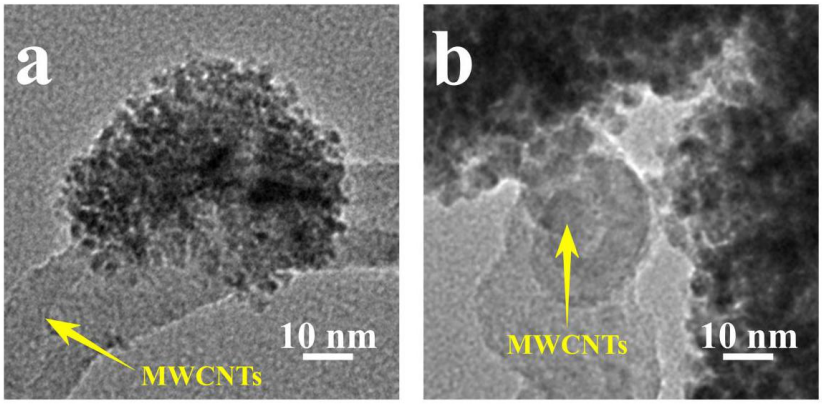

Fig. S11 TEM images of HS-CeO_2/MWCNTs formed in the early periods (a) and HS-CeO_2/MWCNTs (b).

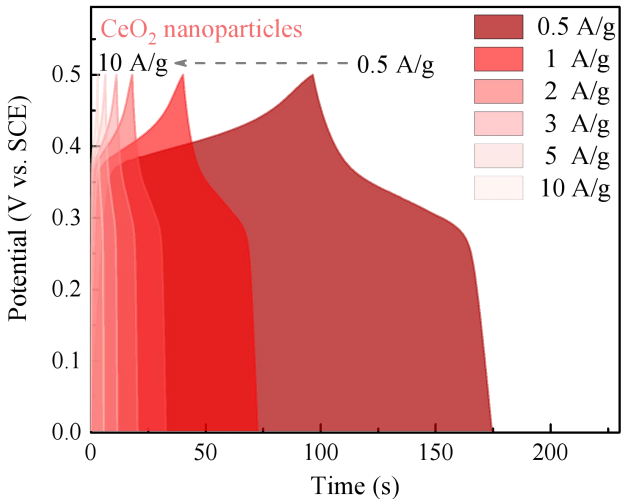

Fig. S12 Galvanostatic charge-discharge profiles of CeO_2 nanoparticles at different current densities.

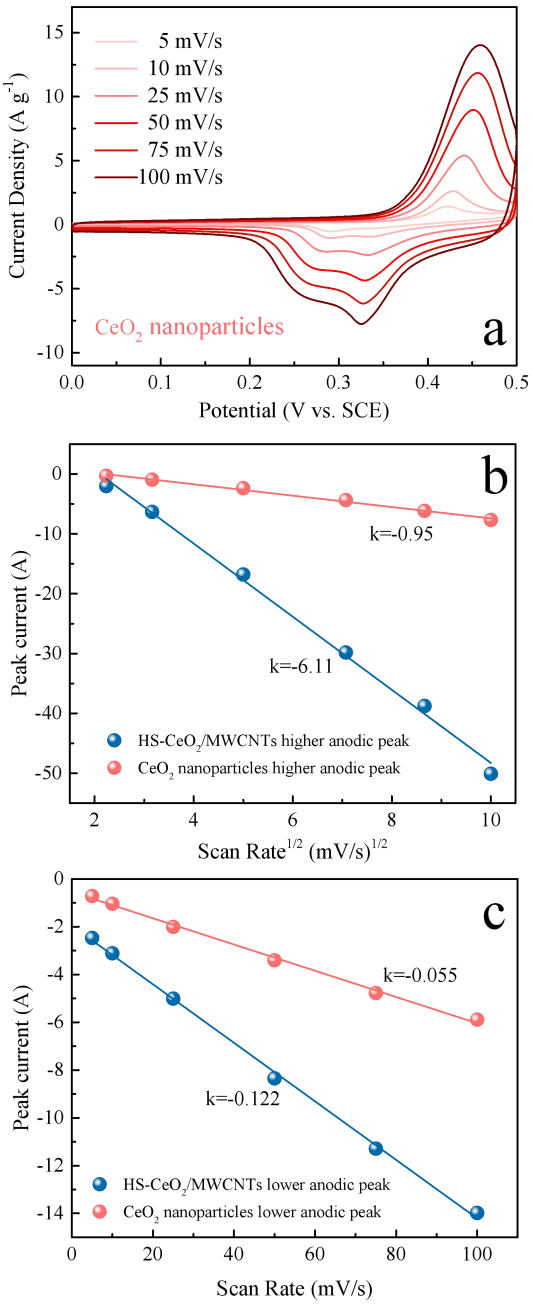

Fig. S13 CV curves of CeO_2 nanoparticles (a); graphs of lower anodic peak currents plotted against $v^{1/2}$ for HS-CeO_2/MWCNTs and CeO_2 nanoparticles (b); graphs of higher anodic peak currents plotted against v for HS-CeO_2/MWCNTs and CeO_2 nanoparticles (c).

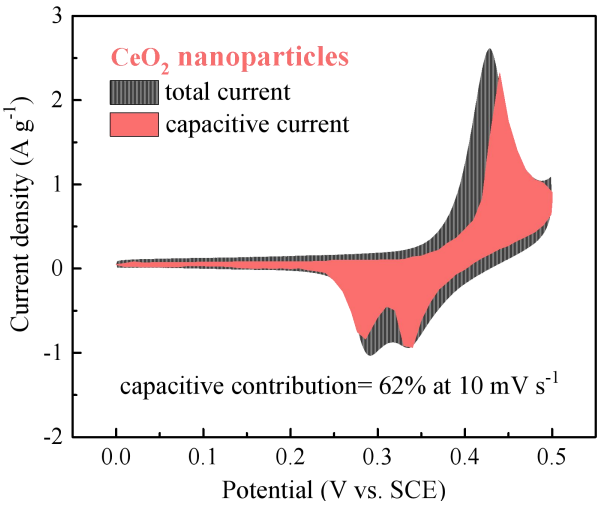

Fig. S14 Capacitive contribution of CeO_2 nanoparticles at 10 mV s^{-1}.

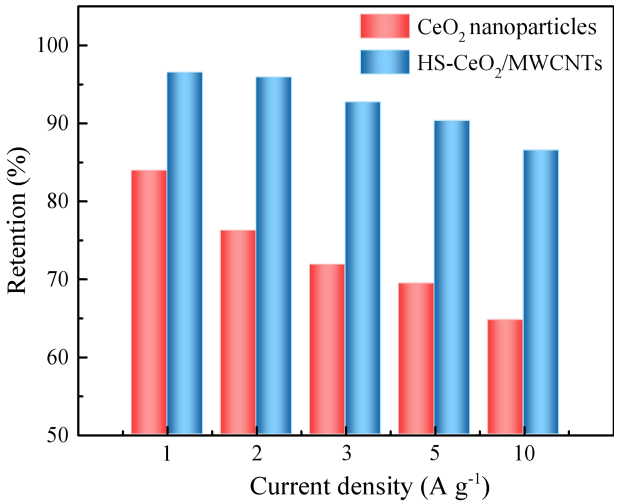

Fig. S15 Rate performance of HS-CeO_2/MWCNTs and CeO_2 nanoparticles.

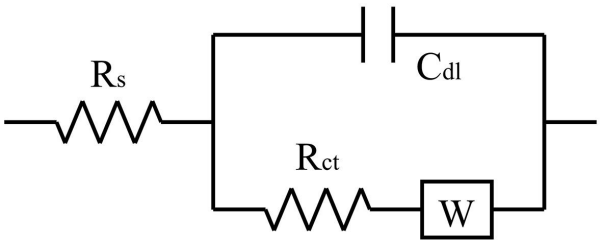

Fig. S16 The simulation equivalent circuit for the the Nyquist plots of HS-CeO_2@MWCNTs and CeO_2 nanoparticles.

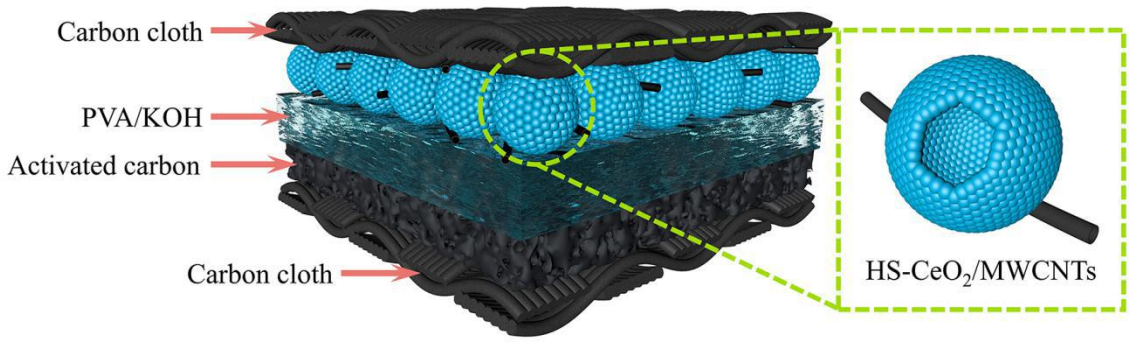

Fig. S17 Schematic representation of the device.

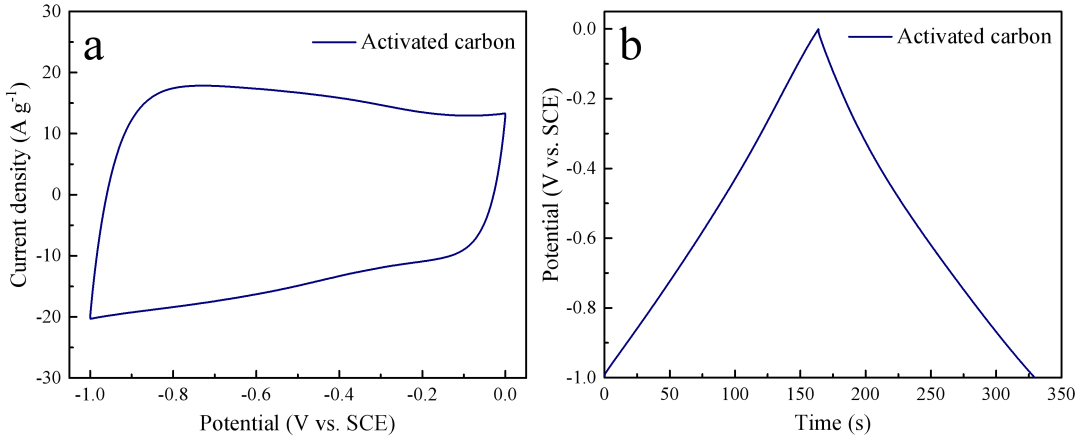

Fig. S18 CV curves of AC at the scan rate of 100 mV s^{-1} (a); galvanostatic charge-discharge profiles of AC at 1 A g^{-1}(b).

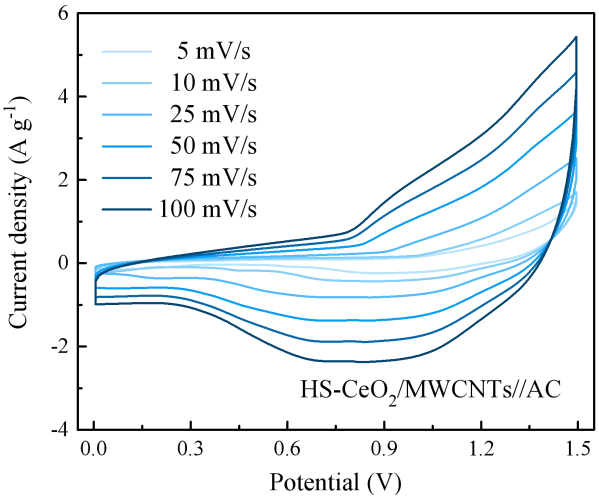

Fig. S19 CV curves of HS-CeO_2/MWCNTs//AC all-solid ASC at various scan rates.

Supplementary Tables

Table S1 Comparison of rate performance for CeO_2 nanoparticles, CeO_2/bare MWCNTs, HS-CeO_2/MWCNTs and CeO_2-coated MWCNTs at varied current density from 0.5 to 10 A g^{-1}.

Sample	Specific capacitance (F g^{-1})						Retention (%)				
	0.5 A g^{-1}	1 A g^{-1}	2 A g^{-1}	3 A g^{-1}	5 A g^{-1}	10 A g^{-1}	1 A g^{-1}	2 A g^{-1}	3 A g^{-1}	5 A g^{-1}	10 A g^{-1}
CeO_2 nanoparticles	78.5	65.9	59.8	56.4	54.5	50.8	83.9	76.2	71.8	69.4	64.7
CeO_2/bare MWCNTs	136.8	123.9	118.2	114.3	110.2	103.6	90.6	86.4	83.6	80.6	75.7
HS-CeO_2/ MWCNTs	450.4	434.6	431.9	417.6	406.9	389.7	96.5	95.9	92.7	90.3	86.5
CeO_2-coated MWCNTs	386.4	371.3	338.2	322.8	305.7	281.7	96.1	87.5	83.5	79.1	72.9

Table S2 Comparison of capacitance values for various structural morphologies of CeO_2 based electrodes.

Materials	Mass loading	Capacitance	Current density or scan rates	Electrolyte	Retention	Ref
RGO/CNT/CeO_2	Glassy carbon electrode	215 F g^{-1}	0.1 A/g	1 M Na_2SO_4	1000 cycles 85%	3
CeO_2 /graphene	2 – 3 mg cm^{-2}	208 F g^{-1}	1 A/g	3 M KOH	-	4
Ceria/Graphene	1 mg cm^{-2}	185 F g^{-1}	2A/g	0.5 M Na_2SO_4	4000 Cycles 94.4%	5
CeO_2/Fe_2O_3	2 mg cm^{-2}	142.6 F g^{-1}	5 mV/s	6 M KOH	1000 cycles 94.8%	6
Nano CeO_2 /AC	-	162 F g^{-1}	2 mA/cm^2	1 M H_2SO_4	1000 cycles 99%	7
RGO/CeO_2	-	265 F g^{-1}	5 mV/s	3 M KOH	1000 cycles 96.2%	8
CeO_2/PPy	8 mg cm^{-2}	193 F g^{-1}	1 A/g	1 M $NaNO_3$	500 cycles 90%	9
(Ce–V) mixed oxide	-	179 F g^{-1}	20 mV/s	1 M $LiClO_4$	-	10
CeO_2 NSs	-	134.6 F g^{-1}	1 A/g	1 M KOH	1000 cycles 92.5%	11
Graphene-ceria	Glassy carbon electrode	110 F g^{-1}	10 mV/s	1 M H_2SO_4	-	12
Hierarchical cerium oxide	5 mg cm^{-2}	235 F g^{-1}	1 A/g	2 M KOH	10000 cycles 91%	13
CeO_2/GO	3 mg cm^{-2}	383 F g^{-1}	3 A/g	6 M KOH	500 cycles 86.05%	14
NiO-CeO_2	1 mg cm^{-2}	305 F g^{-1}	1 A/g	3 M KOH	1000 cycles 91%	15
MnO_2/CeO_2	-	274.3 F g^{-1}	0.5 A/g	3 M KOH	1000 cycles 93.9%	16
CeO_2 nanoparticles	2-3 mg cm^{-2}	97.72 F g^{-1}	1 A/g	3 M KOH	1000 cycles 86.4%	17
CeO_2 nanorods		162.47 F g^{-1}			90.1%	
CeO_2 nanocubes		149.03 F g^{-1}			88.3%	
PANI/5 wt % N,S-GQDs@CeO_2 nanocomposite	1.3 mg cm^{-2}	189 C g^{-1}	1 A/g	1M H_2SO_4	1000 cycles 75 %	18
HS-CeO_2/MWCNTs	5 mg cm^{-2}	450.5 F g^{-1}	0.5 A/g	3 M KOH	5000 cycles 90.1%	This work

Table S3 Comparison of rate performance for HS-CeO_2/MWCNTs and CeO_2 nanoparticles at varied current density from 0.5 to 10 A g^{-1}.

Sample	Specific capacitance (F g^{-1})						Retention (%)				
	0.5 A g^{-1}	1 A g^{-1}	2 A g^{-1}	3 A g^{-1}	5 A g^{-1}	10 A g^{-1}	1 A g^{-1}	2 A g^{-1}	3 A g^{-1}	5 A g^{-1}	10 A g^{-1}
CeO_2 nanoparticles	78.5	65.9	59.8	56.4	54.5	50.8	83.9	76.2	71.8	69.4	64.7
HS-CeO_2/ MWCNTs	450.4	434.6	431.9	417.6	406.9	389.7	96.5	95.9	92.7	90.3	86.5

References

[1] D. Joung, V. Singh, S. Park, A. Schulte, S. Seal, S. Khondaker, *J. Phys. Chem. C*, 2011, **115**, 24494-24500.

[2] B. Xu,Q. T. Zhang, S. S. Yuan, S. X. Liu, M. Zhang,T. Ohno, *Catalysis Today*, 2017, **281**, 135-143.

[3] R. Rajendran, L. K. Shrestha, K. Minami, M. Subramanian, R. Jayavel, K. D. Ariga, *J. Mater. Chem. A*, 2014, **2**, 18480-18486.

[4] Y. C. Wang, X. Guo,J. H. Liu, T. Chen, H. B. Yang, C. M. Li, *Dalton Trans*, 2011, **40**, 6388-6391.

[5] A. S. Dezfuli, M. R. Ganjali, H. R. Naderi, P. Norouzi, *Rsc Advances*, 2015, **5**, 46050-46060.

[6] N. S. Arul, D. Mangalaraj, R. Ramachandran, A. N. Grace, J. I. Han, *J. Mater. Chem. A*, 2015, **3**, 15248-15258.

[7] L. S. Aravinda, K. U. Bhat, B. R. Bhat, *Materials Letters*, 2013, **112**, 158-161.

[8] Z. Y. Ji, X. P.Shen, H. Zhou, K. Chen, *Ceramics International*, 2015, **41**, 8710-8716.

[9] X. Wang, T. M. Wang, D. Liu, J. S. Guo, P. Liu, *Ind. Eng. Chem. Res*, 2016, **55**, 886-894.

[10] I. C.Amaechi, A. C. Nwanya, D. Obi, S. C. Ezugwu, A. E. Udounwa, A B. C. Ekwealor, R. U. Osuji, M. Maaza, F. I. Ezema, *Ceramics International*, 2016, **42**, 3518-3524.

[11] K. Prasanna, P. Santhoshkumar, Y. N. Jo, I. N. Sivagami, S. H. Kang, Y. C. Joe, C. Lee, *Applied Surface Science*, 2018, **449**, 454-460.

[12] T. Saravanan, M. Shanmugam, P. Anandan, M. Azhagurajan, K. Pazhanivel, M. Arivanandhan, Y. Hayakawa, R. Jayavel, *Dalton Trans*, 2015, **44**, 990-998.

[13] G. J. Zeng, Y. Chen, L. Chen, P. X. Xiong, M. D. Wei, *Electrochimica Acta,* 2016, **22**, 773-780.

[14] D. Y. Deng, N. Chen, X. C. Xiao, S. F. Du, Y. D. Wang, *Ionics*, 2017, **23**, 121-129.

[15] N. Padmanathan, S. Selladurai, *Ionics*, 2014, **20**, 409-420.

[16] H. H. Zhang, J. N. Gu, J. Tong, Y. F. Hu, B. Guan, B. Hu, J. Zhao, C. Y. Wang, *Chemical Engineering Journal,* 2016, **286**, 139–149.

[17] A. Jeyaranjan, T. S. Sakthivel, M. Molinari, D. C. Sayle, S. Seal, *Part. Part. Syst. Charact,* 2018, 1800176.

[18] G. Oskueyan, M. M. Lakouraj, M. Mahyari, *Electrochimica Acta*, 2019, **299**, 125-131.